Yeganeh, Maria; Rabensteiner, Samuel; Cheng, Qiang; Ranta, Olli; Karimkashi Arani, Shervin; Kaario, Ossi; Larmi, Martti

Experimental and Numerical Investigation of Hydrogen Jet-Wall Impingement

Published in:
SAE Technical Papers

DOI:
10.4271/2022-01-1009

Published: 30/08/2022

Document Version
Peer-reviewed accepted author manuscript, also known as Final accepted manuscript or Post-print

Experimental and Numerical Investigation of Hydrogen Jet-Wall Impingement

Author, co-author (Do NOT enter this information. It will be pulled from participant tab in MyTechZone)

Affiliation (Do NOT enter this information. It will be pulled from participant tab in MyTechZone)

Abstract

Decarbonization of the automotive industry is one of the major challenges in the transportation sector, according to the recently proposed climate neutrality policies, e.g., the EU 'Fit for 55' package. Hydrogen as a carbon-free energy career is a promising alternative fuel to reduce greenhouse gas emissions. The main objective of the present study is to investigate non-reactive hydrogen jet impingement on a piston bowl profile at different injection angles and under the effect of various pressure ratios (PR), where PR is the relative ratio of injection pressure (IP) to chamber pressure (CP). This study helps to gain further insight into the mixture formation in a heavy-duty hydrogen engine, which is critical in predicting combustion efficiency. In the experimental campaign, a typical high-speed z-type Schlieren method is applied for visualizing the jet from the lateral windows of a constant volume chamber, and two custom codes are developed for post-processing the results. In particular, the jet's major characteristics i.e., penetration, width, and cross-sectional area are calculated at different PRs (25, 10, 5, and 2.5). The results show that higher pressure ratios lead to faster penetration and larger cross-sectional areas of the hydrogen jet. In addition, the jet-piston interaction at different angles as well as the flow around the piston towards the liner and back to the main cylinder volume are studied considering the optimization of mixture formation in the cylinder. By changing the injection angle (10°, 15°, and 20°), jet-piston impingement occurs near the edges, which results in greater hydrogen concentration around those areas, adversely affecting mixture formation. The measurements are further used to validate a numerical model for hydrogen injection and mixing in a similar jet-piston geometry, applying an unsteady Reynolds-averaged Navier-Stokes simulation approach in the commercial software Star-CCM+.

1. Introduction

Global warming has become a central issue in the past decades since fossil fuels are still the main power supply in the transport sector, which is one of the main polluting sectors in energy production [1]. Fossil fuel combustion produces a huge amount of greenhouse gases (CO_2 and H_2O) which has led to more stringent emissions legislation e.g., the EU 'Fit for 55' package. One possible option for transition to zero carbon emission is utilizing alternative fuels e.g., hydrogen for powering transportation.

Hydrogen has been advanced as an energy carrier to produce motive power in internal combustion engines over numerous benefits. Wide range of flammability limit (fuel fraction in air = 4-75 (%-vol.)), low ignition energy (0.02 mJ), low quenching distance (0.64mm), high flame velocity (1.86 m/s), and high octane rating (>130) are advantages that motivate investment in hydrogen as a carbon-free energy carrier [2]. Apart from benefits related to lowering local pollution and CO_2emissions, hydrogen internal combustion engines (H_2ICEs) can be flex-fuel, produced affordably in large quantities, and tolerant of fuel impurities [2]. Several studies [4-7] have also shown that with the possibility of retrofitting engines, introducing H_2ICEs are relatively easy.

In the context of H_2ICEs, direct injection (DI) seems more promising compared to port fuel injection (PFI). Although in PFI, the long mixing time and subsequent higher uniformity of the fuel can result in higher part-load efficiency, it possesses a low power output because hydrogen occupies a large fraction of the intake volume [8,9]. Moreover, there is more tendency for backfire and engine knocking in PFI H_2engines [10,11]. On the contrary, DI can not only restrict backfire and engine knocking but also can provide higher specific power [12]. In DI engines, one of the principal parameters, which can directly affect the combustion quality, is fuel-air mixing and mixture formation which mainly depends on the gas jet characteristics [13]. Hence, investigating those characteristics i.e., jet penetration, width, and cross-sectional area under the effect of dominant variables (i.e., pressure ratio (PR) and injection angle) is an indispensable part of combustion optimization of H_2DI engines.

The PR defines how fast the compressed hydrogen gas expands into the chamber and sets the limit between sub-sonic and super-sonic injection. For supersonic injection the flow inside the nozzle becomes choked, i.e., the velocity inside the nozzle is sonic and the mass flow stays constant while decreasing the chamber pressure at a constant injection pressure. Still, higher PR leads to higher turbulence levels and faster mixing, which makes this parameter particularly interesting for DI engines. In addition, the location and the angle of the injection might serve as parameters for improving the mixture formation, especially when the gas jet interacts with engine walls such as the piston bowl and the liner. It is important to understand how much the location of the injector (center-mounted or side-mounted) and its angle can affect the mixing and combustion quality.

The research questions raised above are to be addressed in this paper by investigating the effect of PR on the H_2 gas jet penetration, width, and cross-sectional area both experimentally and numerically. Additionally, the effect of injection angle on the jet-piston interaction will be studied. Apart from the fact that experiments provide new data to validate CFD simulation results, the novelty of the work can be noted as applying a newly designed gas jet injector with a single-hole cap and investigating the effect of the injection angle. The outline of the paper is as follows. In section 2 (methodology), the experimental setup, image post-processing, and simulation basics are explained. Then, section 3 presents the effect of variables, i.e., pressure ratio and injection angle on the H_2 jet characteristics based on both experiments and CFD simulation results. Finally, the main conclusions of the jet characteristics are acquainted in section 4.

2. Methodology

In this section, the experimental setup and its components, optical system, test matrix, image post-processing method, and CFD simulation basics are described, respectively.

2.1 Experimental Setup

A constant volume chamber was used for gas jet measurements in the experimental campaign. The chamber was connected to the hydrogen fuel tank and to the nitrogen bottle rack (to be pressurized). Due to the high chamber pressures and related safety issues, the injector (a solenoid outwardly opening gas injector with a single-hole cap of 5mm diameter from BOSCH) was mounted on top of the chamber. Hence, the jet visualization was through the quartz lateral windows of the chamber. Since the chamber was designed so that the injector could only be mounted on the top center and vertically, investigating the effect of the injection angle was done by placing a sample of a piston bowl profile with different angles at the bottom. The captured images could be rotated later for comparing the experiments and CFD simulation results. Other components of the experimental setup were the pressure sensor, temperature sensor, release valve, and control system (LabVIEW software and driver from National Instrument) for synchronizing the injector and high-speed color camera (Photron fastcam SA-Z). The software was also connected to the pressure and temperature sensor to monitor the injection pressure, chamber pressure, and temperature, as well. Figure 1 shows the experimental setup, injector, and the inside view of the chamber.

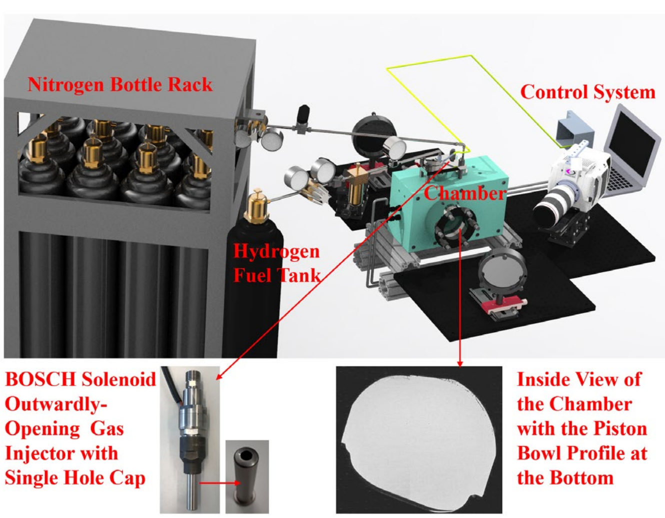

Figure 1. Experimental setup, injector, and the inside view of the chamber.

2.2 Optical System

A typical high-speed z-type schlieren imaging was applied for the jet visualization. Schlieren is a non-intrusive method to capture transparent fluid flows and relies on the fact that light rays are bent whenever they encounter density differences. Thus, since the hydrogen was injected into the chamber which was filled with nitrogen and there was also a difference between the injection pressure and chamber pressure, schlieren imaging seemed to be a promising option to visualize the jet. As shown in Figure 2, first, the jet is illuminated by a collimated light beam from a high-power monochromatic LED spotlight and the first parabolic mirror. Then, the jet refracts the light. After that, the second mirror concentrates the light beam into the lens of the high-speed camera located behind an iris to partly block the refracted light and generate the schlieren image. Table 1 provides more detailed information on the optical system, as well. It should be also noted that due to the limitations of the size of lateral windows (considering safety issues) and the focal length of the parabolic mirrors, it was not possible to visualize the whole view of the chamber especially when the gas jet behavior near the edges was desired. Hence, the measurements were done once to get the right-hand side view and another time to get the left-hand side view.

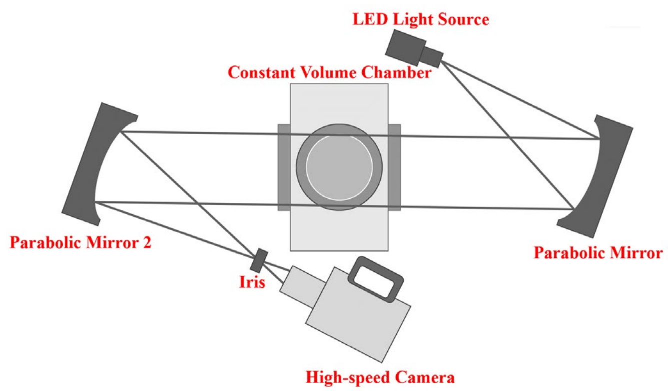

Figure 2. The high-speed z-type schlieren imaging system.

Table 1. Optical system components.

Component	Feature
Electrical Power of the LED	21W
Focal Length of the First Mirror	609,6 mm
Focal Length of the Second Mirror	762 mm
Percentage of the Knife-edge Cut-off	Approximately 60 %
Frame Rate	40000 fps
Resolution	768x640

2.3 Experimental Test Matrix

The jet penetration, width, and cross-sectional area are the main jet characteristics that were measured at 12 test points under the effect of pressure ratio (PR=2.5, 5, 10, and 25) at different injection angles or piston bowl profiles with different angles (10°, 15°, and 20°). It is important to note that the jet characteristics were measured in the free penetration phase (until the time step at which the jet just hits the wall or piston bowl profile). After that, the jet-wall impingement was investigated qualitatively to be compared with CFD simulation results for analyzing the mixing behavior. All measurements were performed at a constant injection pressure (IP=25 bar) and injection duration (3ms) at standard room pressure (1atm) and temperature (295K). Therefore, the variation of pressure ratio was by changing the chamber pressure (CP= 1, 2.5, 5, and 10 bar). In addition, each test point was repeated 20 times to ensure the accuracy of the data. As the jet-to-jet variations would definitely affect the late simulation calibration, image similarity analysis was also done to ensure that this number of repetitions is enough for validating the simulations.

Table 2. Experimental test matrix.

Variable	Pressure Ratio	Injection Pressure (bar)	Chamber Pressure (bar)	Injection Angle (°)
Case 1	2,5	25	10	10
	5	25	5	10
	10	25	2.5	10
	25	25	1	10
Case 2	2,5	25	10	15
	5	25	5	15
	10	25	2.5	15
	25	25	1	15
Case 3	2,5	25	10	20
	5	25	5	20
	10	25	2.5	20
	25	25	1	20

2.4 Image post-processing

As mentioned earlier, the hydrogen jet image sequences were captured via high-speed schlieren imaging. For post-processing, two steps were done: (1) merging the right and left-hand side of the jet and doing the image similarity analysis with a custom Python code and (2) calculating the jet characteristics (penetration, width, and cross-sectional area) by a custom MATLAB program.

The Python code was developed in two versions. The first version was for merging the images of the jet's left and right-hand sides for each repetition of each test point, separately. This was to obtain the jet characteristics plots with error bars related to jet-to-jet variation. The second version was developed to average the images of the jet's left and right-hand sides for all 20 repetitions of each test point to compare mixing between the experiments and simulations. Since the CFD simulations were RANS-based, it was necessary to calculate the average image of the 20 repetitions. Figure 3 shows a sample of a combined image for one repetition versus a sample of a combined average image of 20 repetitions at the same time step.

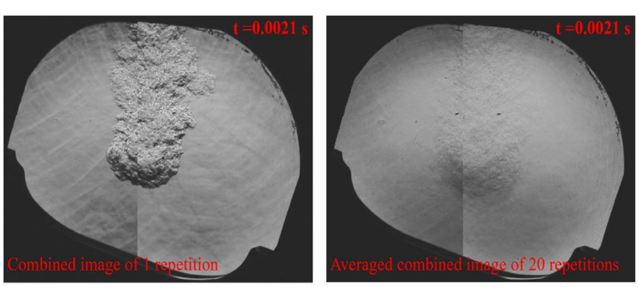

Figure 3. A combined image of 1 repetition versus a combined average image of 20 repetitions at the same time step.

The same python code for averaging also contains a part for analyzing the image similarity between each repetition image and the averaged image to ensure that 20 repetitions are enough for validating the CFD simulations. The structural similarity index metric (SSIM) was applied and showed a range of image similarity between 0.83 and 0.99 which seems promising for acceptable consistency between the experiments and the simulations. As shown in Figure 4, the image similarity gradually decreases in the jet's penetration phase and has its minimum value when the jet-wall impingement just happens. Since the SSIM is based on the pixels' grayscale and the largest difference between pixels' grayscale is related to the impingement phase where the jet mainly shows the random turbulence, the decreasing trend of the image similarity is logically expected.

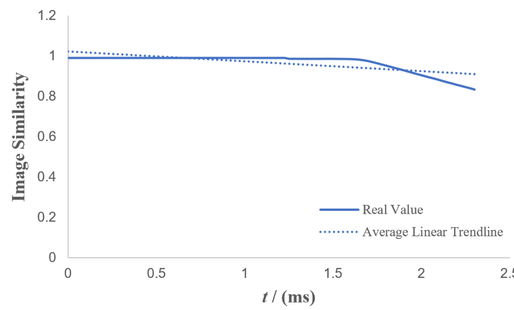

Figure 4. Image similarity analysis based on SSIM in the jet's free penetration phase

For calculating the jet penetration, width, and cross-sectional area, a MATLAB code was developed which follows the steps shown in Figure 5. As observed, first, the code produces the magnitude image and subtracts its background. Then, it starts filling the holes of the jet because it expects that there are no holes inside the jet. After that, the code removes the shadows and the small objects from the image. Finally, the code traces the boundaries of the jet by following the selected threshold value.

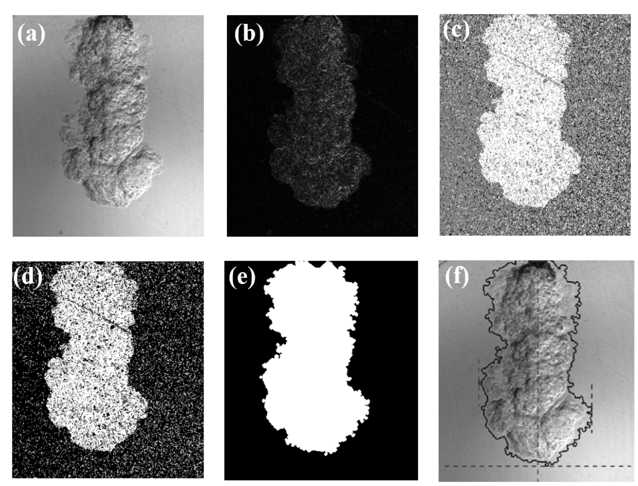

Figure 5. MATLAB code steps for calculating the jet characteristics. (a) raw image, (b) magnitude image, (c) subtracted magnitude image, (c) binary image, (d) denoise image, (e) final image with jet edge detection.

2.5 Error Analysis

There were four main origins of errors in the experimental campaign. First, there is at least 1 bar pressure drop before the injector valve during the injection and also some internal pressure losses just before the nozzle e.g., in the space between the valve and the cap which means the pressure ratios in the test matrix are nominal values, and the real values are less than the nominal values. Second, the accuracy of injection and chamber pressure gauges were ± 0.5% of full-scale output accuracy. Third, the jet penetration, width, and cross-sectional area calculations cover up to 95 % of the maximum axial penetration of the jet. In other words, the error in the accuracy of tracking the jet boundaries is 5%. Last, the jet-to-jet variation error which is shown with error bars in the plots of jet characteristics in the results section and tried to be addressed by repeating each experiment 20 times to ensure the accuracy of the data.

2.6 CFD Simulation Methods

Unsteady Reynolds-Averaged Navier-Stokes (URANS) simulations of supersonic hydrogen injection were conducted in the commercial software Star-CCM+. The URANS approach was chosen, as this project is conducted in the context of an industrial application, where many simulations with different stimulation parameters are conducted and the computational power and time are limited. The current setup with a segregated flow solver and the k-ωSST Menter turbulence model was previously tested and validated by the authors [14]. In this work, comparisons with high-resolution LES simulations by Vuorinen et al [15] (nitrogen as injected gas) and experimental measurements of single-hole hydrogen injection in a constant volume chamber were conducted. The results showed that the high Reynolds number flow and the supersonic shock structures can be closely represented with the present model at an appropriate mesh resolution for the tested nozzle pressure ratios ranging from 2 to 8.5 Also, a mesh-dependency study was conducted in [14], with five different mesh resolutions in the near nozzle region ranging from 2 cells per nozzle diameter to 32 cells per nozzle diameter. This led to the result that a grid resolution of at least 8 cells per nozzle diameter is needed in the near nozzle region to capture the shock structure and geometrical development (jet penetration, width, and cross-sectional area). The Redlich-Kwong real gas law (like in e.g. [16]) is used to account for compressibility of the gas. More details on the solvers and turbulence models can also be found in [14].

A full 3-dimensional model of the test chamber with the piston profile, as presented in Figure 6 (a), is utilized in the simulations and the computational domain is divided into two separate regions, namely the injector and the chamber. This way, the same model can later be used in simulations of the full engine cycle, where the injector region can be removed after the injection to simplify further computations.

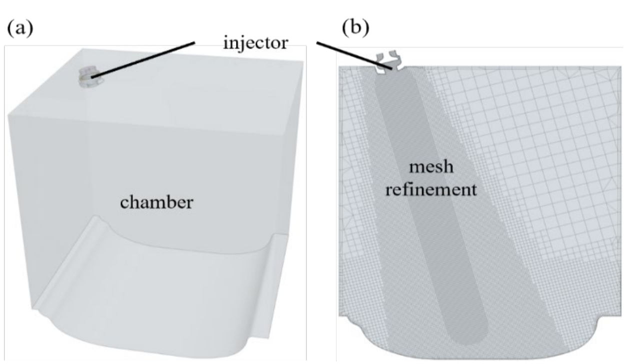

Figure 6. (a) CFD geometry consisting of the piston profile, the injector, and the side walls. (b) The mesh refinement levels in the regions, where high flow velocities are expected.

Simulation of the full internal injector geometry, including the transient valve opening, is a complicated task, which requires a very high mesh resolution and additional computational power, as the characteristic dimensions of the injector are typically orders of magnitude smaller than that of the chamber or cylinder. Furthermore, capturing the supersonic flow in the near-nozzle region requires high resolution and low time steps. Therefore, in an industrial context using a simplified injector model instead of including the full internal injector geometry is a viable option. Previous simplification approaches include the application of a boundary condition at the location of the Mach disk (the normal shock that forms due to the supersonic flow after the nozzle exit) [17] or just before the nozzle hole [18]. Another option is to cut out a region close to the injector and simulate this region with a high fidelity LES approach, which can then be applied as a boundary condition for simulation of the whole domain [16,19].

In the present case, a single-hole cap is used on top of a hollow cone injector, and to capture the flow in the cap, the inlet boundary is set just before the hollow cone nozzle, as presented in Figure 7. The inlet boundary pressure is ramped up during the simulation to model the transient wall opening and the inlet pressure curves were obtained from 1-dimensional simulations of the whole injector. An interface between the injector and chamber region is set at the location of the valve seat, which can be deactivated when the injector is closed. In our preliminary simulations, this approach led to superior results compared to a more simplified injection model, in which the inlet boundary was set right before the single-hole nozzle. The present setup is therefore a compromise between accuracy and computational efficiency as the flow in the injector, upstream of the inlet boundary, and the transient valve opening are not explicitly simulated. For more details on the boundaries, the authors refer to [14].

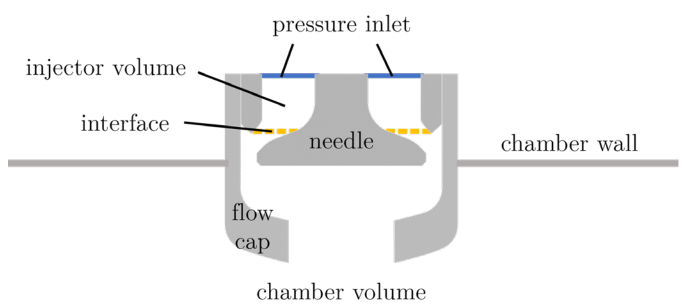

Figure 7. A pressure boundary is used to model the transient valve opening and closing of the hollow cone injector. The boundary is also set to include the dynamics in the flow cap and the interface can be deactivated to separate the regions when the valve is closed.

In the preliminary simulations, it was found that at least 8 cells per nozzle diameter are necessary to approximately capture the near-nozzle shock structure, which defines the mixing and development of the gas jet further downstream. In the present case, 16 cells were used over the diameter of D=5 mm, which corresponds to a cell size of about 0.3 mm. The fine mesh resolution in the nozzle is kept in the cylindrical near-nozzle region and the diameter and length of which are set to 3D and 22.5D, respectively. Additionally, two levels of cone-shaped refinement and refinement in the piston bowl are used to cover the relevant flow areas, while the coarse background mesh is quickly recovered in the rest of the domain, which is shown in Figure 6 (b). The initial conditions in the chamber were set according to the experiments where T_{ch}=295 K, P_{ch}=1, 2.5, 5, 10 bar, and air (23 %-wt. oxygen, 77 %-wt. nitrogen) is the background gas. The walls were treated as adiabatic and no-slip. In the injector region, the initial temperature and pressure are equal to the chamber and the injector is considered to be filled with H_2.

3. Results and Discussion

In this section, the geometrical development of the free jet is utilized to study the effect of pressure ratio (PR) and to validate the numerical model until the jet-wall impingement. Further, the flow along the piston wall is visually compared between the simulation and the experiments for different injection angles. As only limited numerical information is available from the experimental measurements, the simulations are then used to investigate the initial fuel distribution and mixing after the jet-wall impingement.

3.1 Effect of pressure ratio on the hydrogen jet characteristics in the free penetration phase

One of the most substantial parameters which can highly affect the jet characteristics is the pressure ratio (PR). It is the ratio of the injection pressure (IP) to the chamber pressure (CP). In this study, the PR is varied by changing the chamber pressure (CP = 1, 2.5, 5, and 10 bar) at a constant injection pressure (IP = 25 bar) because the injector is designed so that the highest possible injection pressure is 25 bar. The effect of PR on different jet characteristics (penetration, width, and cross-sectional area) in the free penetration phase up until the time that the jet just impinges the wall (or piston bowl profile) is compared between the experiments and the simulation.

Figure 8 (a) shows the effect of different pressure ratios (PR=2.5, 5, 10, and 25) on the jet penetration. At higher pressure ratios, the pressurized hydrogen gas expands faster into the chamber, leading to higher velocities after the inlet and accordingly faster penetration as long as the injection pressure is constant, higher pressure ratios are related to lower chamber pressures which means that the drag against jet expansion is decreasing and assisting the penetration. The faster jet penetration can also have a positive influence on mixing as it leads to early impingement on the piston, followed by a recirculating motion towards the cylinder head. Since the jet cross-sectional area is an important representative of efficient mixing, the effect of the pressure ratio on this parameter is also investigated in Figure 8 (b). Rising the pressure ratio leads to an increase in the jet cross-sectional area and hence, a better mixture formation.

(a) (b)

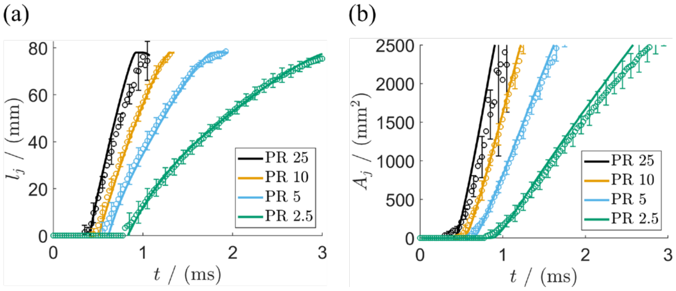

Figure 8. Effect of pressure ratio (PR) on the jet penetration length for experimental schlieren measurements (∘ with error bars) and URANS simulations (solid line). For the comparison, the zero point was set to the position where the jet enters the observation window in the experiment.

Figure 8 also shows that for both jet penetration and cross-sectional area, the simulations are in good agreement with the experiments. The largest discrepancy between the simulation and the experiments is found for the highest pressure ratio (PR=25), which could be both due to the weak schlieren signal and the relatively worse cell resolution for the higher near nozzle velocities. Another important point, which can be seen in this figure, is that for different pressure ratios, the jet penetration starts at different time steps. This can be explained by the effect of chamber pressure on the needle opening. As expected, higher chamber pressures cause a delay in the needle opening and slower initial jet development. Therefore, the latest starting point of the penetration is related to the highest chamber pressure (CP=10) or the lowest pressure ratio (PR=2.5). The same scenario applies to the plots of the jet width and cross-sectional area versus time, as well.

The consistency between the experiments and the simulation seems at first glance slightly worse for the jet width, as shown in Figure 9 (a). Especially for PR of 5 and 10, the simulated results are at the lower end of the experimental range for the width, while the penetration and cross-sectional area are in very good agreement. An explanation is that in the experiments, the jet tends to create side branches in the boundary region which cannot be represented in the URANS simulations, due to their average character. The reason for the presence of the side branches might be needle vibration, turbulence, and pressure inhomogeneity in the chamber or in the jet. Figure 9 (b) shows a sample of such a branched jet, which influences the maximum jet width but neither penetration nor cross-sectional area because the branches are located behind the jet tip and the additional area might be balanced by a dip in another place. As mentioned earlier, there is a difference between a single measurement and the average outcome of the experiments (Figure 3).

(a) (b)

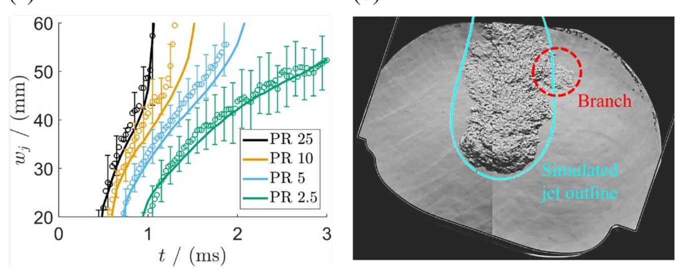

Figure 9. (a) The effect of pressure ratio (PR) on the jet width for experiments (∘ with error bars) and URANS simulations (solid line). (b) An example of a branched jet that is not possible to be modelled in simulations. It is found that generally, the simulated jet width is slightly lower than the experimental values as the simulated jet is an average representation, which does not capture momentary phenomena, such as side branches in the experiments.

A possible indicator for the potential mixing of the hydrogen is the volume average of the turbulent kinetic energy

$$k_T = \frac{1}{2}\overline{u_i' u_i'} \qquad (1)$$

which is defined as the root mean square of the fluctuating components of the flow velocity u_i' and which relates to the level of turbulent mixing. Due to the faster expansion and the respective higher velocities, the turbulence increases with the PR, as shown in Figure 10 (a). During the injector opening k_T increases quickly. For the highest PR (25bar), a clear maximum can be found, corresponding to the time when the hydrogen jet exits the piston and the flow along the piston-wall becomes quasi-steady. For lower PRs the local maximum is less clear, but it is observed that k_T reaches a plateau at the corresponding time. To show the effect of faster jet development and higher turbulence levels on mixing, the volume uniformity of the hydrogen mass fraction $\widetilde{m}_{\mathrm{H}_2}$ for different PR is compared in Figure 10 (b). Here, the uniformity index (UI) of a quantity ϕ is defined as

$$UI_\phi = 1 - \frac{\sum_n |\bar{\phi} - \phi| V_n}{2|\bar{\phi}| \sum_n V_n}, \qquad (2)$$

where V_n is the volume of cell n.

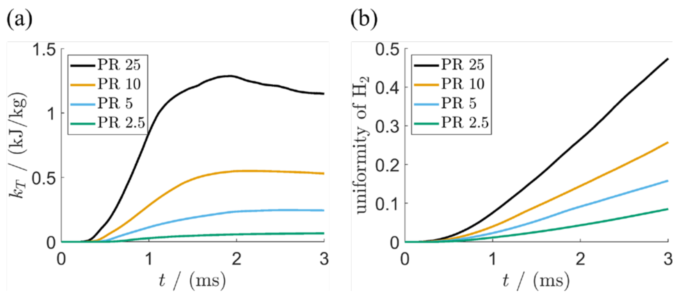

Figure 10. Effect of pressure ratio on the mixture formation by (a) the volume average kinetic energy and (b) hydrogen uniformity.

Figure 10 also indicates that the fuel uniformity increases with higher PRs. In the present study, the advantage of high PRs is providing fast mixing because of the choked nozzle condition. As shown in Figure 11, the flow is choked at PR=25, 10, and 5 and for PR= 2.5, the steady-state mass flow is about 2 g/s lower which is not choked anymore. Since the theoretical limit for the choked flow of hydrogen at 300 K lies at a PR =1.89 [20], the higher limit in the present case is explained. However, as mentioned earlier in the error analysis section, for PR= 2.5, although the nominal value is 2.5, the real value is smaller because the PR is defined as the ratio between chamber pressure (CP) and the upstream bottle pressure before the injector (IP). Therefore, the effective ratio between the chamber pressure (CP) and the pressure right before the nozzle is lower due to the internal pressure losses in the injector.

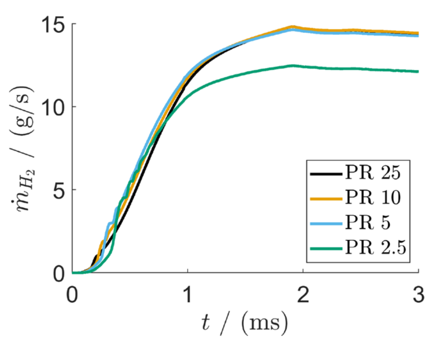

Figure 11. The hydrogen mass flow is nearly the same for PR= 25, 10, and 5 due to the choked flow from the nozzle. For PR=2.5, the steady-state mass flow is lower, indicating that this case is not choked.

3.2 Effect of injection angle on the mixture formation in the impingement phase

Since one additional challenge of the automotive industry in developing a new generation of H_2ICEs is the location and the angle of the injection especially when the injector is side-mounted it was attempted to study the effect of the injection angle on the gas jet behavior. However, due to the high chamber pressures, the safety issue did not allow us to change the location and the angle of the injector. As a solution, piston bowl profiles with three different angles were placed at the bottom of the chamber for observing the effect of the injection angle and jet-wall impingement. By following this idea, the captured frames from the experiments can be rotated and compared with the results of CFD simulations.

As explained earlier, schlieren imaging is sensitive to density differences. Hence, a possible strategy for validating the simulations is to compare the density gradient of the numerical results with the averaged results of the 20 experimental runs. A challenge with obtaining the jet boundary, especially in the early stages of injection is posed by the pressure waves, which can be observed in Figure 12 (a). This view shows the logarithm of the absolute density gradient $\log|\nabla\rho|$. To tackle this challenge the jet outline is instead obtained from the field of the hydrogen mass fraction ($\widetilde{m}_{H_2}$), as shown in Figure 12 (b). The threshold of $\widetilde{m}_{H_2} = 0.001$ is found by visual comparison to the density gradient field and the resulting jet outline can then be compared to the measurement data, as presented in panel (c) of the figure.

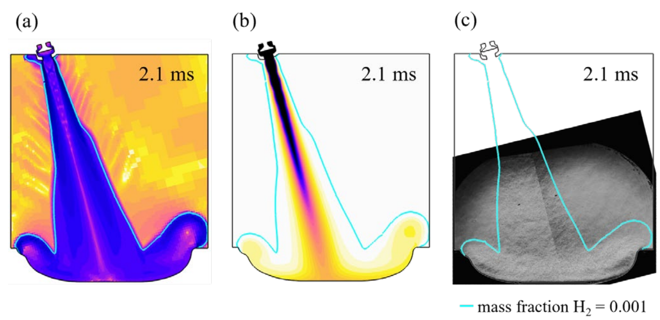

Figure 12. The hydrogen jet boundary from the simulations can be obtained from (a) the pressure gradient field or (b) the mass fraction of hydrogen. (c) A comparison of the simulated hydrogen jet boundary (blue line) with the density gradient field in the schlieren image.

Figure 13 shows the injection angle effect on the mixing behavior. At 15°, the jet-wall impingement takes place near the center of the piston bowl profile, while at 10° and 20° it is closer to the left and right edge, respectively. The good correspondence between the experiments and the simulations during the free jet development (until about 1.3 ms after the start of injection (SOI)) was already shown in the previous section. Also, for the flow along the piston bowl, the simulation results are validated by the experiments. However, a slightly faster jet development is observed at the latest time step (2.5 ms) in the numerical simulations. In general, it could be desirable for a uniform mixture of the fuel to spread uniformly through the piston bowl and recircle symmetrically back towards the cylinder head. In this respect, the case with the injection angle of 20° does not lead to a preferable outcome. As can be observed, at 1.7 ms the fuel starts to exit from the piston bowl on the right, while it is still in the central flat part on the left. This leads to a high hydrogen concentration along the liner on the right side at 2.5 ms, which could lead to an asymmetrical final fuel distribution and fuel in the piston crevice at the corresponding location.

For 10° and 15° the fuel spreads through the piston bowl more symmetrically. While the jet hits closest to the piston centre for 15° injection angle, the jet outline at 2.5 ms after SOI indicates that the fuel recirculates more symmetrically. Hence, predicting the mixing efficiency is quite complicated while there are signs of symmetric fuel distribution in both 10° and 15° cases. Additionally, the recirculating jet on the left side can interact with the incoming gas flow from the piston, which is an interesting effect that could increase mixing by creating additional turbulence in both of these cases.

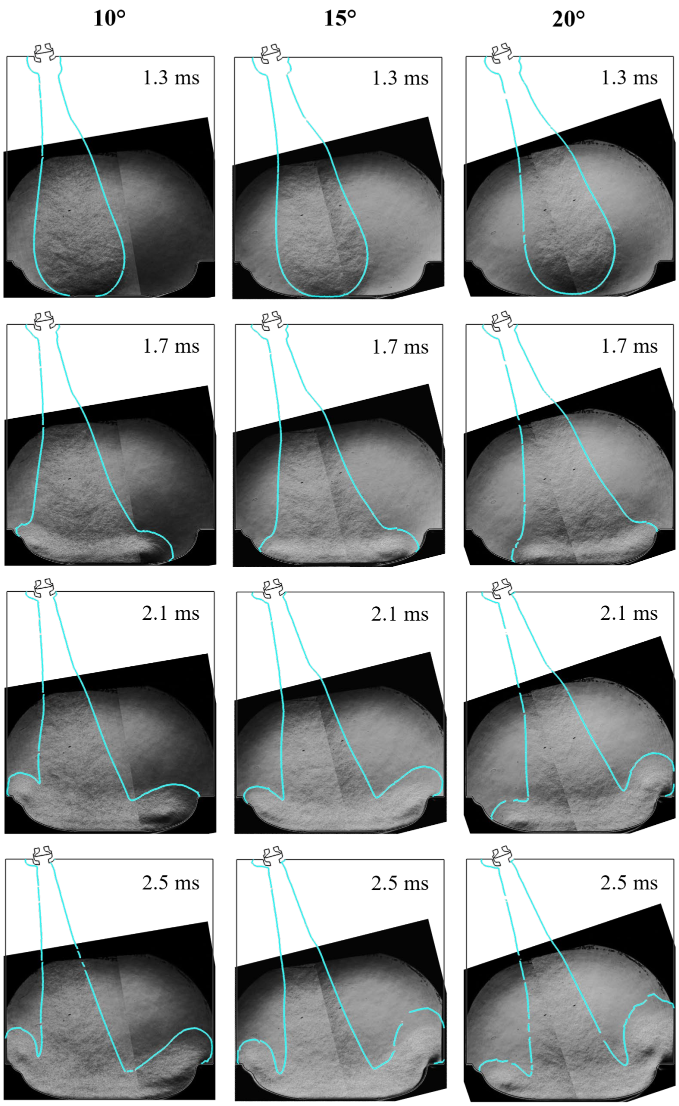

Figure 13. Comparison of numerical results (blue line) and the average density gradient field from 20 measurement runs for three different time injection angles at four time steps.

Since the observations from Figure 13 are purely qualitative, one possible way for investigating the effect of injection angle is introduced here by means of the fuel-balance (β_{H_2}) between the left and right side of the cylinder. This parameter is the volume integral of the hydrogen mass density (ρ_{H_2}) weighted with the x-axis position x (left-right in the present view, with zero at the piston centre and left as the negative direction) and normalized by the total injected mass of hydrogen (M_{H_2}) and the piston radius (R),

$$\beta_{H_2} = \frac{1}{M_{H_2} R} \int_V \rho_{H_2} x \, dV. \qquad (3)$$

The new fuel balance parameter, introduced in the above equation, ranges between -1 and $+1$, where the limits correspond to the cases where all the fuel is either at the left or right chamber wall and a balanced case in $\beta_{H_2} = 0$. Together with the uniformity, this parameter can give information about the mixture quality during the early stages of the fuel mixing, such as found in the present case.

For the three different injection angles, the fuel balance starts at about -0.85 as the jet begins penetration from the injector nozzle. As presented in Figure 14, β_{H_2} then quickly rises for all three cases, with the smallest slope for 10° injection angle. After 3 ms both 10° and 15° injection angles show a rather balanced fuel distribution with values of -0.06 and 0.15, respectively. However, for 20° injection angle, β_{H_2} reaches about 0.35 indicating that a clearly higher amount of fuel is present on the right chamber side, as was expected from the qualitative inspection of Figure 14. Therefore, according to the fuel balance results, the smaller injection angles (10° or 15°) seem more promising than 20° for a better mixture formation. However, further studies including the piston motion and longer mixing times are needed to make a final conclusion. Overall, the experimental investigations offer a good validation of the numerical model and some preliminary hints on the preferred injection angle.

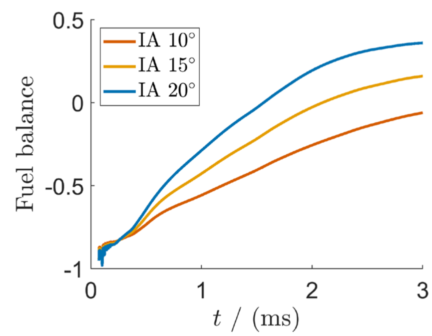

Figure 14. The fuel balance parameter which describes the left-right distribution of the fuel with the zero point at the piston center. It is an indicator of early stage mixing and tendencies for the final mixture distribution.

4. Conclusion

This paper presents an experimental and numerical (URANS simulation) investigation of hydrogen jet dynamics. The jet characteristics (penetration length, width, and cross-sectional area) are studied under the effect of pressure ratio (PR = 2.5, 5, 10, and 25) by changing the chamber pressure at constant injection pressure. The effect of the injection angle on the mixture formation is studied, as well. The main conclusions are as follows:

1. The geometric jet characteristics from the experiments can be competently reproduced with the present URANS simulation approach. Except for the jet width, the jet penetration and cross-sectional area from the experiments are well-matched to the simulations. The width of the jet is typically higher in the experiments because of some side branches in the jet boundaries due to the needle vibration, turbulence, or pressure inhomogeneity in the chamber. However, these random shapes of the jet in the experiments, are not possible to be modeled numerically because of the average character of the simulations.

2. The pressure ratio represents the pressure differences between the injection pressure and chamber pressure. Typically, a larger pressure ratio means more pressure drop from the hydrogen jet to the ambient gas. Therefore, a longer jet axial penetration and radial width, as well as a larger cross-sectional area can be observed which is a prime representative of efficient mixing. The results show that a ~50% increase in the pressure ratio leads to ~50% increase in the jet penetration, width, and cross-sectional area. Higher pressure ratios can also increase turbulence levels and turbulent mixing, leading to higher uniformity of the mixture, which is desirable in many engine applications.

3. The choked flow phenomenon was observed at the PR>2.5 due to the pressure ratio exceeding the theoretical limit of the choked flow of hydrogen at 300 K (PR=1.89). In PR=2.5, the real value of the pressure ratio is slightly smaller than the choked flow limit due to the pressure losses before and after the injector's valve. Thus, the injected mass is quite similar at different PRs except for PR=2.5.

4. The jet-piston interaction can be satisfactorily represented with the numerical model and is only slightly faster in the simulations. Although the schlieren measurement results are purely qualitative, calculations of the fuel balance parameter in the simulations were performed to check which angles are most promising for efficient mixing. Preliminary considerations suggest that smaller injection angles (10° or 15°) might lead to the most balanced final mixture, avoiding high fuel concentrations at one side of the piston.

5. Overall, the results of this study show that pressure ratios over 5 (PR≥ 5) seem more promising for a better mixture formation. In addition, jet-wall impingement investigations indicate that injection angles in the range of 10º - 15º will avoid dense hydrogen areas near the edges of the piston bowl profile which can assist in efficient mixing, as well.

References

1. European Environment Agency (EEA), "Greenhouse gas emissions from transport," https://www.eea.europa.eu/data-and-maps/indicators/transport-emissions-of-greenhouse-gases/transport-emissions-of-greenhouse-gases-12, accessed Apr. 2022.
2. White, C.M., Steeper, R.R., Lutz, A.E., "The hydrogen-fuelled internal combustion engine: a technical review," International Journal of Hydrogen Energy, 31(10):1292-1305, 2006, doi: 10.1016/j.ijhydene.2005.12.001.
3. Verhelst, S., "Recent progress in the use of hydrogen as a fuel for internal combustion engines," International Journal of Hydrogen Energy, 39(2): 1071-1085, 2014, doi:10.1016/j.ijhydene.2013.10.102.
4. Iwasaki, H., Shirakura, H., and Ito, A., "A Study on Suppressing Abnormal Combustion and Improving the Output of Hydrogen Fueled Internal Combustion Engines for Commercial Vehicles," SAE Technical Paper 2011-01-0674, 2011, doi:10.4271/2011-01-0674.
5. Dennis, P., Dingli, R., Abbasi Atibeh, P., Watson, H. et al., "Performance of a Port Fuel Injected, Spark Ignition Engine Optimised for Hydrogen Fuel," SAE Technical Paper 2012-01-0654, 2012, doi:10.4271/2012-01-0654.
6. Natarajan, S., Abraham, M., Rajesh, M., Subash, G. et al., "DelHy 3W - Hydrogen Fuelled Hy-Alfa Three Wheeler," SAE Technical Paper 2013-01-0224, 2013, doi:10.4271/2013-01-0224.
7. Huyskens, P., Van Oost, S., Goemaere, P., Bertels, K. et al., "The technical implementation of a retrofit hydrogen PFI system on a passenger car," SAE Technical Paper 2011-01-2004, 2011, doi:10.4271/2011-01-2004.
8. Luo, Q., Hu, J., Sun, B., Liu, F., et al, "Effect of equivalence ratios on the power, combustion stability and NOx controlling strategy for the turbocharged hydrogen engine at low engine speeds," International Journal of Hydrogen Energy, 44(31): 17095-17102, 2019, doi: 10.1016/j.ijhydene.2019.03.245.
9. Wang, X., Sun, B., Luo, Q., "Energy and exergy analysis of a turbocharged hydrogen internal combustion engine," International Journal of Hydrogen Energy,44(11): 5551-5563, 2019, doi:10.1016/j.ijhydene.2018.10.047.
10. Duan, J., Liu, F., Sun, B., "Backfire control and power enhancement of a hydrogen internal combustion engine," International Journal of Hydrogen Energy, 39(9): 4581-4589, doi:10.1016/j.ijhydene.2013.12.175.
11. Luo, Q., Sun, B., "Inducing factors and frequency of combustion knock in hydrogen internal combustion engines," International Journal of Hydrogen Energy, 41(36): 16296-16305, doi:10.1016/j.ijhydene.2016.05.257.
12. Yamane, K., "Hydrogen Fueled ICE, Successfully Overcoming Challenges through High Pressure Direct InjectionTechnologies: 40 Years of Japanese Hydrogen ICE Research and Development," SAE Technical Paper 2018-01-1145, 2018, doi:10.4271/2018-01-1145.
13. Wang, X., Sun, B., Luo, Q., Bao, L., et al, "Visualization research on hydrogen jet characteristics of an outward-opening injector for direct injection hydrogen engines,", Fuel, 280 (118710), 2020 doi:10.1016/j.fuel.2020.118710.
14. Rabensteiner, S., "Modelling of supersonic hydrogen jets," M.Sc. thesis, Mechanical Engineering Department, Aalto University, 2021.
15. Vuorinen, V., Yu, J., Tirunagari, S., Kaario, O. et al., "Large-eddy simulation of highly underexpanded transient gas jets," *Physics of Fluids* 25(1):016101, 2013, doi:10.1063/1.4772192.
16. Deshmukh, A. Y., Falkenstein, T., Pitsch, H., Khosravi, M. et al., "Numerical Investigation of Direct Gas Injection in an Optical Internal Combustion Engine," *SAE International Journal of Engines*, 11(6):1447–1478, (2018), doi:10.4271/2018-01-0171.
17. Mather, D.K., and Reitz, R.D., "Modeling the Effects of Auxiliary Gas Injection on Diesel Engine Combustion and Emissions", SAE Technical Paper 2000-01-0657, 2002, doi:10.4271/2000-01-0657.
18. Keskinen, K., Kaario, O., Nuutinen, M., Vuorinen, V. et al. "Mixture formation in a direct injection gas engine: Numerical study on nozzle type, injection pressure and injection timing effects," *Energy*, 94:542–556, 2016, doi:10.1016/j.energy.2015.09.121
19. Deshmukh, A. Y., Vishwanathan, G., Bode, M., Pitsch, H. et al., "Characterization of Hollow Cone Gas Jets in the Context of Direct Gas Injection in Internal Combustion Engines,". SAE Technical Papers 2018-01-0296, 2018, doi:10.4271/2018-01-0296.
20. Yip, H. L., Srna, A., Yuen, A. C. Y., Kook, S. et al., "A review of hydrogen direct injection for internal combustion engines: Towards carbon-free combustion," *Applied Sciences (Switzerland)*, 9(22): 4842, 2019, doi:10.3390/app9224842

Contact Information

Maryam Yeganeh
M.Sc.
Doctoral Candidate
Aalto University
School of Engineering
Department of Mechanical Engineering
Research Group of Energy Conversion
Mail: P.O.Box 14300, FI-00076 Aalto, Finland
Visiting address: Sähkömiehentie 4, 02150 Espoo
Phone: +358505747731
e-mail: maryam.yeganeh@aalto.fi

CRediT authorship contribution statement

Maryam Yeganeh: Investigation, Software, Formal analysis, Visualization, Writing – original draft, Writing – review & editing. Samuel Rabensteiner: Conceptualization, Software, Visualization, Writing – original draft Writing – review & editing. Qiang Cheng: Conceptualization, Investigation, Software, Supervision, Writing – review & editing. Olli Ranta: Conceptualization, Investigations, Software. Shervin Karimkashi: Resources, Writing – review & editing. Ossi Kaario: Resources, Supervision, Writing – review & editing. Martti Larmi: Supervision, Funding acquisition, Writing – review & editing.

Acknowledgments

This work was supported by the AGCO power company as a preliminary stage in developing a hydrogen heavy-duty engine. Special thanks to Senior Technician Jarno Järvinen, M.Sc. Otto Blomstedt, and B.Sc. Juho Kuusela-Opas for technical assistance and mechanical design. The authors want to acknowledge the computational resources provided by the Aalto Science-IT project for performing the simulation and to thank the Triton team for their advice.

Definitions/Abbreviations

PR	Pressure Ratio
IP	Injection Pressure
CP	Chamber Pressure
H_2ICE	Hydrogen Internal Combustion Engine
DI	Direct Injection
PFI	Port Fuel Injection
H_2DI	Hydrogen Direct Injection
CFD	Computational Fluid Dynamics
URANS	Unsteady Reynolds Averaged Navier Stokes
UI	Uniformity Index
SSIM	Structural Similarity Index Metric
SOI	Start of Injection